2026 IEEE International Conference on Robotics and Automation (ICRA 2026)
June 1-5, 2026. Vienna, Austria

HybNetic: A Mobile Hybrid Magnetic Actuation System

Lukas Masjosthusmann, Nicholas R. Posselli, and Sarthak Misra

***Abstract*— Magnetic actuation enables contactless control of medical microrobots and instruments and offers the potential for improved safety and effectiveness in robot-assisted minimally invasive surgery. While much research is being conducted on the development of surgical devices, there is a lack of external actuation systems that provide the necessary magnetic field shaping capability for *in vivo* control. Existing magnetic actuation systems often face trade-offs between field shaping capability and workspace size. In this work, we introduce HybNetic, a mobile hybrid magnetic actuation system that combines a single electromagnet with four independently rotatable permanent magnets mounted on a robotic arm. The C-shaped configuration of HybNetic has an opening of 520 mm, allowing positioning around the human torso. The mobility of the employed robotic arm extends the effective workspace to the length of a human body. We describe the design and field modeling and characterize the magnetic performance by comparing analytical model predictions and finite element simulations with experimental validations. Finally, we demonstrate the versatility of HybNetic by levitating a magnetic sphere and navigating a magnetic guidewire through a dimensionally accurate phantom of the abdominal aorta. The demonstrations highlight the potential of HybNetic as a magnetic actuation system with a workspace that is suitable for *in vivo* manipulation of macro- and micro-scale magnetic devices.**

I. INTRODUCTION

Minimally invasive surgery (MIS) offers reduced patient trauma, shorter recovery times, and fewer complications [1], [2]. Robot-assisted MIS combines the benefits of MIS with the dexterity and precision of robotic platforms. Recent research has focused on developing new actuation methods that enable safe and controllable manipulation of surgical instruments inside the human body. Magnetic actuation has emerged as one of the most promising approaches [3].

Magnetic actuation enables contactless control of both tethered and untethered magnetic devices. In endovascular procedures, magnetically steered tethered robots have demonstrated the potential to increase reachability while minimizing the risk of tissue damage [4]. In the gastrointestinal tract, capsule robots have been magnetically guided to enhance diagnostics and therapy [5]. At a smaller scale, magnetic microrobots access deep-seated regions of the lung or brain that conventional MIS cannot reach, enabling targeted delivery of therapeutic agents [6].

External magnetic actuation systems (EMAS) provide the fields required to control magnetically actuated surgical devices and microrobots. EMAS can be broadly categorized into electromagnet-based and permanent-magnet-based systems. Coil arrays surrounding the workspace can generate complex fields with high flexibility and have been successfully demonstrated in small-scale *in vitro* and *ex vivo* studies [7], [8], [9]. However, scaling multi-coil systems to human-sized workspaces is difficult, as integration into current clinical workflows can restrict patient access and disrupt standardized procedures. In addition, generating sufficiently strong fields at a larger scale requires high currents, which result in substantial heat generation and high power consumption [10].

Coil configurations with fewer, physically larger coils that partially surround the workspace have been developed as more compatible designs for clinical integration, but these systems inherently produce anisotropic magnetic fields [11]. Mobile single- and multi-coil systems mounted on robotic

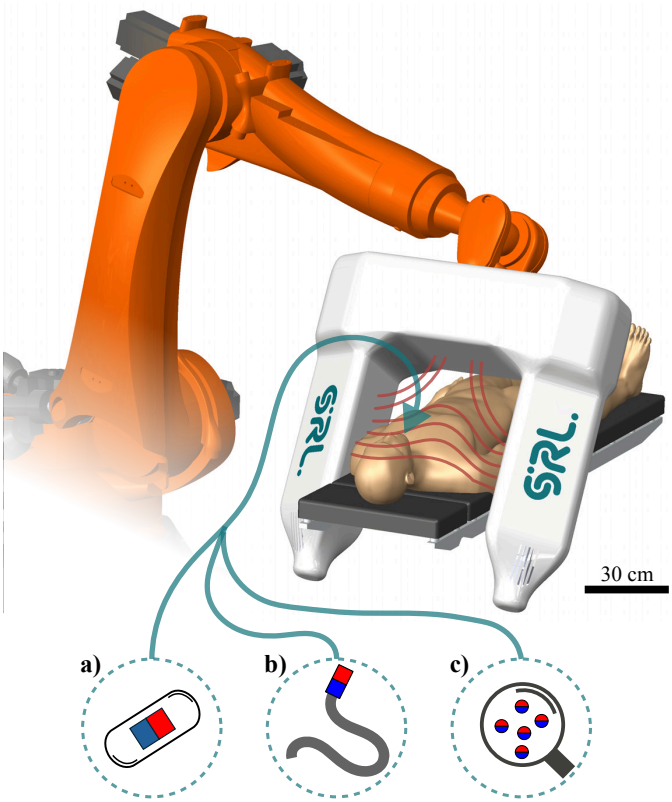

Fig. 1: Schematic illustration of HybNetic: A mobile hybrid magnetic actuation system. HybNetic can be used for clinical interventions. The red lines represent the magnetic field. **a)** Magnetic capsule robots, **b)** Magnetic catheters and endoscopes, and **c)** Magnetic microrobots.

This work was supported by the European Union's Horizon Europe Research and Innovation Programme under Grant Agreement #101070066 (project RĔGO).

All authors are affiliated with Surgical Robotics Laboratory, Department of Biomechanical Engineering, University of Twente, 7522NB Enschede, The Netherlands {l.masjosthusmann, nick.posselli, s.misra}@utwente.nl.

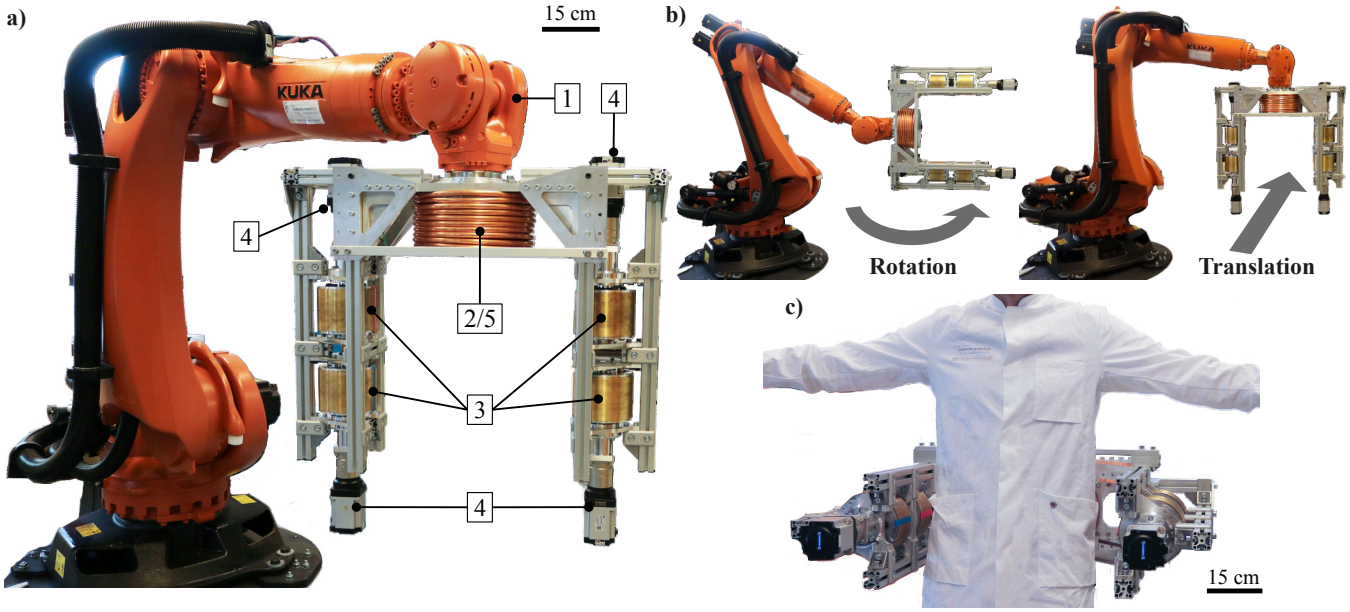

Fig. 2: a) Display of the key components of HybNetic: 1 Robotic arm 2 Coil with iron core 3 Custom-made permanent magnets 4 Electric motor-gearbox combinations 5 Spiral cooling pipe. **b)** Flexible positioning of the system through rotational and translational movements. **c)** HybNetic surrounding a male torso.

arms have been introduced as an alternative to stationary systems, allowing re-orientation of the coils to adjust the magnetic field [12], [13], [14]. However, the performance is defined by the load capacity of the robotic arms, which can limit the achievable field strengths in larger workspaces.

Permanent-magnet-based systems generate magnetic fields without continuous power input. Arrays of multiple rotating magnets have been explored for field shaping, although over small working areas [15], [16]. The most common design approach consists of a robotic arm carrying a single permanent magnet, providing controllable actuation in human-scale environments [17], [18]. Multi-arm systems, with each robot arm carrying an individual magnet, have been proposed to improve field shaping compared to single-magnet setups [19], [20]. The coordination of more than two mobile magnets in close proximity is inherently difficult due to mutual interactions, which limits the scalability of actuation approaches based on multiple mobile permanent magnets in human-scale settings.

In this work, we present HybNetic, a mobile hybrid magnetic actuation system compatible with human torso–sized workspaces (Fig. 1). Unlike prior systems, HybNetic combines a single electromagnet with four individually rotatable permanent magnets arranged as opposing pairs on a robotic arm. The system can be positioned freely around the torso and supports continuous intraluminal manipulation along the full body length through natural orifices. Within this workspace, HybNetic provides three-dimensional field control, including rotating fields in arbitrary directions and multi-directional force generation. By combining the mobility of the robot arm with the hybrid field-shaping approach, HybNetic can manipulate both macro- and micro-scale magnetic devices in human-scale workspaces.

This paper presents the design, modeling, and actuation capabilities of HybNetic. We describe a model that superposes fields from the electromagnet and the rotating permanent magnets while accounting for the mobility of the system. The magnetic capabilities of the system are characterized using an analytical model and finite element simulations and validated experimentally. Finally, we demonstrate the general functionality and versatility of HybNetic by levitating a magnetic sphere and steering a magnetic guidewire through a dimensionally accurate abdominal aorta phantom.

II. Design of a Mobile Hybrid Magnetic Actuation System

HybNetic is a magnetic actuation system designed to manipulate tethered and untethered magnetic devices in *in vivo* compatible workspaces. Its working principle is based on the interaction between an externally generated magnetic field and the magnetic moment of a magnetic device. This interaction results in an acting force ($\mathbf{F} \in \mathbb{R}^3$) and torque ($\mathbf{T} \in \mathbb{R}^3$), which together are referred to as a magnetic wrench:

$$\mathbf{W} = \begin{pmatrix} \mathbf{F} \\ \mathbf{T} \end{pmatrix} = \begin{pmatrix} \nabla(\mathbf{m} \cdot \mathbf{B}(\mathbf{p})) \\ \mathbf{m} \times \mathbf{B}(\mathbf{p}) \end{pmatrix}, \tag{1}$$

where $\mathbf{m} \in \mathbb{R}^3$ is the magnetic moment of the target and $\mathbf{B} \in \mathbb{R}^3$ the magnetic field at position $\mathbf{p} \in \mathbb{R}^3$. For tethered robots, torque-based steering is preferable to force-based steering because field gradients decay faster than the field itself, allowing torque-based control to remain more effective over larger distances. Nevertheless, the capability to apply forces to microrobots can improve the performance of torque-based locomotion methods [21] and increase the range of possible

applications. Consequently, a torque-oriented actuation approach is prioritized for HybNetic, but complemented by the ability to generate forces sufficient to lift magnetic targets.

A. System Configuration

HybNetic comprises four independently rotatable permanent magnets and a single coil arranged in a symmetric C-shaped configuration mounted on a robotic arm (Fig. 2a)). The system employs a hybrid actuation concept that combines permanent magnets and an electromagnet to leverage the advantages of both approaches while mitigating their individual limitations [22]. Electromagnet-based systems capable of generating three-dimensional magnetic fields in human-scale workspaces require substantial electrical power, on the order of up to multiple tens of kilowatts [3]. In contrast, permanent magnets provide static magnetic fields without continuous energy input and are therefore more energy-efficient. However, the sole use of a static permanent magnet as a field source limits controllability. The magnetic field produced by a permanent magnet is determined by its orientation and distance to the workspace, rather than by a directly adjustable control input such as current. As a result, changing the generated field at a given position requires mechanical rotation or relative displacement.

The symmetric arrangement of four rotating permanent magnets around the workspace of HybNetic preserves the energy efficiency of permanent magnets while enabling flexible field control. Rotating a single magnet allows directional control of the magnetic field in a plane, while the field magnitude at a given position remains fixed for a given distance and orientation. Arranging two individually rotatable permanent magnets as a pair increases the controllability through magnetic field superposition. Coordinated rotation of the two magnets allows control of both the direction and magnitude of the resulting magnetic field in two spatial directions. Placing two pairs symmetrically around the workspace further increases controllability. The magnetic field generated by one pair can be increased or partially compensated by the opposing pair, enabling the generation of local near-zero fields and bidirectional magnetic force application.

Extending the rotating permanent magnet concept to control the magnetic field in the remaining spatial direction would require additional pairs of magnets. Such an extension would increase structural complexity and compromise the partially surrounding configuration that enables flexible positioning and orientation of HybNetic relative to the cylindrical workspace. Therefore, the magnetic field component in the remaining spatial direction is primarily generated by an electromagnet, which provides direct field control without obstructing the open workspace design.

The open C-shaped configuration of HybNetic provides a cylindrical workspace with a diameter of 520 mm, covering up to 95% of the bi-deltoid shoulder widths and hip widths of Dutch males, [23], which is sufficient for *in vitro* experiments with human-sized phantoms (Fig. 2c)). The reach of the robotic arm extends the effective workspace of the system, enabling continuous actuation across the entire length of the human body (Fig. 2b)). In addition, the mobility of the robotic arm allows for flexible repositioning of the system to shape the magnetic field or to adapt to a surgical procedure. The weight of the system, excluding the robotic arm, is approximately 210 kg, which corresponds to the load capacity limit of the KR 210 R2700 prime robotic arm (KUKA AG, Germany) used. By combining both the rotating permanent magnets and the electromagnet, HybNetic is designed to generate magnetic fields up to 50 mT at the workspace center and rotating fields with arbitrary orientation. These capabilities enable torque-based steering of tethered continuum robots and actuation of untethered micro-scale devices in human-sized workspaces.

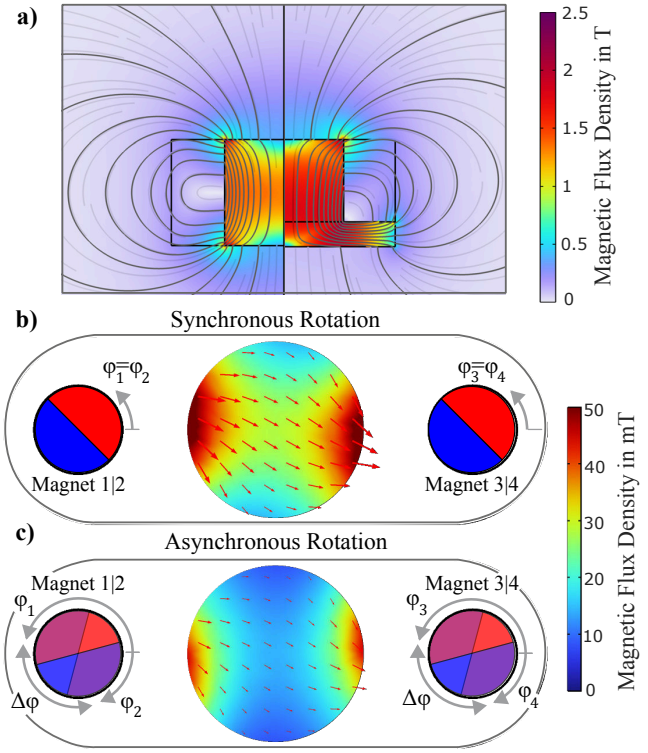

Fig. 3: HybNetic uses an electromagnet and four permanent magnets. **a)** Comparison of the magnetic field generated for two different core shapes: cylindrical core (left side) and core with back plate (right side), both evaluated at an identical input power of 6000 W and a total system weight of 65 kg. **b)** Synchronous field control mode: Orientation of all magnets (φ_i with $i \in [1, ..., 4]$)) is identical. **c)** Asynchronous field control mode: Orientation of each magnet is individually controlled and the orientation difference within a pair ($\Delta\varphi = \varphi_{1,3} - \varphi_{2,4}$) is nonzero.

B. Field Optimized Electromagnet

A single central electromagnet, driven by a servo driver (DPCANIE-040A400, Advanced Motion Controls, USA), controls the magnetic field along the direction of the rotational axes of the permanent magnets. The electromagnet features an iron core (ALLIEDPUREIRON, PURON Metals, Germany) and is surrounded by a spiral copper pipe connected to a water-cooling system to support continuous operation. The design of the electromagnet is optimized using finite element methods (FEM) to maximize the magnetic

field generated while adhering to the allocated weight limit of 65 kg for the electromagnet (COMSOL Multiphysics 6.2, Sweden).

Two coil-core configurations are evaluated. The first follows a conventional design, where the coil length equals the core length, with an optimal inner-to-outer diameter ratio of 0.53 [12]. The second design employs an iron backplate to reduce the reluctance of the magnetic circuit [9], [24]. This results in a maximum magnetic flux density of approximately 32 mT at an axial distance of 250 mm at 6000 W, which is up to 25% higher than the conventional design with identical weight and power input. In addition, the relationship between the resulting magnetic flux density and the input current is analyzed, showing linear behavior, simplifying control of the field generated by the electromagnet. We therefore adopt the backplate design for HybNetic to maximize the power-to-field ratio while minimizing the thermal load.

C. Rotating Permanent Magnets

A core feature of HybNetic is the use of rotating permanent magnets to actively control the magnetic field without having to reposition the magnets. The system incorporates four independent actuation units, each built around a custom-made, diametrically magnetized cylindrical magnet (NdFeB, grade N52H, X-Mag Inc., China) coupled to a motor-gear assembly. Each magnet has a diameter of 150 mm, a length of 108 mm, a weight of 15 kg, and is enclosed in a 2 mm thick brass housing to protect the surface and improve mechanical integrity. According to the FEM model, the four magnets collectively generate fields of up to 32 mT in the x-direction and 19 mT in the y-direction at the center of the workspace.

Each magnet is driven by a synchronous motor with an optical encoder and a rated torque of 3.18 Nm through a planetary gear with a 15:1 ratio. The four actuation units are arranged in two symmetrical pairs, enabling two operating modes for controlling the magnetic field: synchronous and asynchronous . In synchronous mode (Fig. 3b)), all magnets have the same direction and rotate in synchrony, providing direct control of the field direction while maintaining maximum field strength. In asynchronous mode (Fig. 3c)), intentional angular offsets ($\Delta\varphi \in [0, 180]^\circ$) between the magnets cause partial field cancellation, enabling control of the field magnitude at a target location. By combining both modes, HybNetic achieves independent control of the magnetic field strength and direction within the workspace.

III. MODELING

HybNetic is developed for the controlled manipulation of magnetic devices, which requires an accurate prediction of the magnetic field within the workspace. This field is inherently non-homogeneous, resulting from both the central electromagnet and multiple permanent magnets. Moreover, because the magnetic sources are mounted on a robotic arm, the global position and orientation of the system directly influence the local field at any evaluation point. In the following, we first describe the models for the coil and permanent magnets individually, and then combine them into a unified hybrid model that accounts for their spatial configuration and actuation variables.

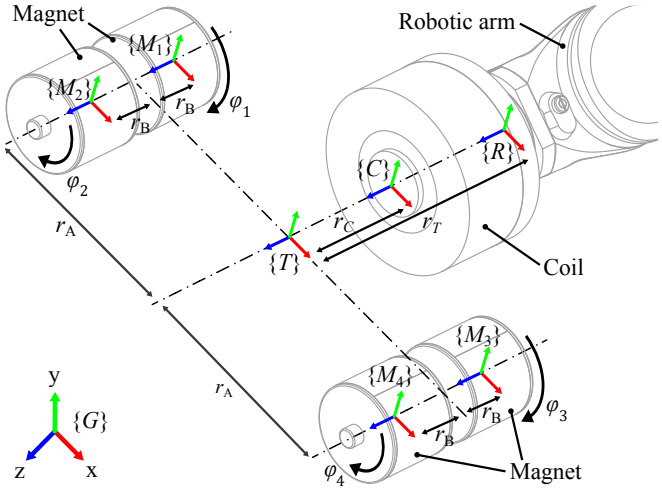

Fig. 4: Overview of the kinematic framework. The global frame ($\{G\}$) is fixed at the base of the robotic arm, and the workspace frame ($\{T\}$) is centered in the C-shaped structure. Each magnetic source has a local frame ($\{M_k\}$ with $k \in [1, ..., 4]$) with its z-axis aligned to $\{T\}$. The fixed distances are $r_a = 10, \text{mm}$, $r_C = 30, \text{mm}$, and $r_B = 40, \text{mm}$.

A. Model of a Single Coil

Finite element simulations (COMSOL Multiphysics 6.2, Sweden) show that the soft iron core remains unsaturated up to a current of 20 A. Under this assumption, the magnetic field $\mathbf{B}_C \in \mathbb{R}^3$ scales linearly with the coil current ($I \in \mathbb{R}$) [7], which simplifies the modeling. We therefore define a position-dependent current-normalized field distribution $\hat{\mathbf{B}}_C(\mathbf{p})$, which can be obtained either numerically or by fitting an analytical function [25]. The field for a current (I) at the target position ($\mathbf{p} \in \mathbb{R}^3$) is then given by

$$\mathbf{B}_C(I, \mathbf{p}) = I\hat{\mathbf{B}}_C(\mathbf{p}). \tag{2}$$

This normalized distribution is later combined with the permanent magnet models under the principle of superposition to describe the total field of our hybrid actuation system.

B. Model of a Single Rotating Permanent Magnet

The permanent magnets are large relative to the intended workspace and positioned in direct proximity to it. In the central region, where the magnet-to-point distance exceeds twice the minimum-bounding-sphere radius, a dipole approximation can be considered accurate [26]. Closer to the magnet, this approximation deteriorates. Therefore, we describe the field with a truncated multipole expansion [27]:

$$\mathbf{B}_M(\mathbf{r}, \mathbf{m}) = \left(\frac{\mu_0}{4\pi||\mathbf{r}||^3}\Gamma_1(\hat{\mathbf{r}}) + \frac{\mu_0}{4\pi||\mathbf{r}||^5}\Gamma_2(\hat{\mathbf{r}}) + \frac{\mu_0}{4\pi||\mathbf{r}||^7}\Gamma_3(\hat{\mathbf{r}}) + \dots \right) \mathbf{m}. \tag{3}$$

where $\mathbf{r} = \mathbf{p} - \mathbf{p}_M$ is the displacement from the magnet center $\mathbf{p}_M$ to the target position, $\hat{\mathbf{r}} = \mathbf{r}/||\mathbf{r}||$, and $\mathbf{m} \in \mathbb{R}^3$ is the

magnetic moment. The matrices Γ_i are geometry-dependent and derived from the shape of the magnet and the direction of its magnetization. They enable us to incorporate the effects of the cylindrical geometry, diametric magnetization, and the six axial through-holes along the circumference [26]. In practice, we truncate the expansion after the first three terms, which improves accuracy compared to the dipole model while remaining computationally efficient for real-time field prediction and control.

C. Model of the Hybrid Actuation System

The total magnetic field generated by the hybrid actuation system is obtained by summing the individually modeled contributions of the coil and permanent magnets, using the principle of superposition [27]. We define a global frame ($\{G\}$) fixed at the base of the robotic arm, and a mobile workspace frame ($\{T\}$) located at the center of the C-shaped structure. The single electromagnet is assigned a local frame ($\{C\}$), while each permanent magnet has a local frame ($\{M_k\}$, with $k \in [1, ..., 4]$). Frame $\{C\}$ is aligned with frame $\{T\}$ with the origin shifted by a fixed offset $\mathbf{r}_c$ along the shared z-axis, coinciding with the coil's magnetization direction and positioning it on the core surface. Each magnet frame ($\{M_k\}$) is located at the center of the corresponding magnet, with its z-axis aligned to the z-axis of the workspace and its x-axis pointing along the diametric magnetization. The angle between the x-axis of magnet k and the x-axis of frame $\{T\}$ is the motor controlled angle φ_k. The translational offset ($\mathbf{r}_k$) between frame $\{T\}$ and frame $\{M_k\}$ is fixed by design. The coil primarily controls the magnetic field along the z-direction of frame $\{T\}$, while the permanent magnets provide control in the xy-plane.

The target position ($\mathbf{p}$) is specified in the global frame, and can be expressed relative to the frame of each source using homogeneous transformations:

$$\mathbf{p}_L = \mathbf{T}_T^L \, \mathbf{T}_G^T \, \mathbf{p}_G, \tag{4}$$

where $\{L\}$ refers to either the coil frame ($\{C\}$) or a magnet frame ($\{M_k\}$). The magnetic field contribution of each source is modeled in the source's frame. By combining the contributions of all magnets and the coil, the total magnetic field can be expressed in $\{G\}$ as:

$$\mathbf{B}_G = \mathbf{R}_T^G \left(\sum_{k=1}^{n} \mathbf{R}_{M_k}^T \mathbf{B}_{M_k}^s + I \cdot \mathbf{R}_C^T \hat{\mathbf{B}}_C \right). \tag{5}$$

Thus, the total field can be compactly expressed as a function of the control variables of the system:

$$\mathbf{B}_G = \mathbf{B}_G(\mathbf{p}_G, \mathbf{q}_{arm}, I, \varphi_k), \tag{6}$$

which represents HybNetic's hybrid actuation approach. The robot arm controls the global position and orientation of the workspace, while the coil and rotating magnets enable local control of the field strength and direction. Equations (1) and (6) serve as the basis for estimating wrenches acting on magnetic targets within the workspace.

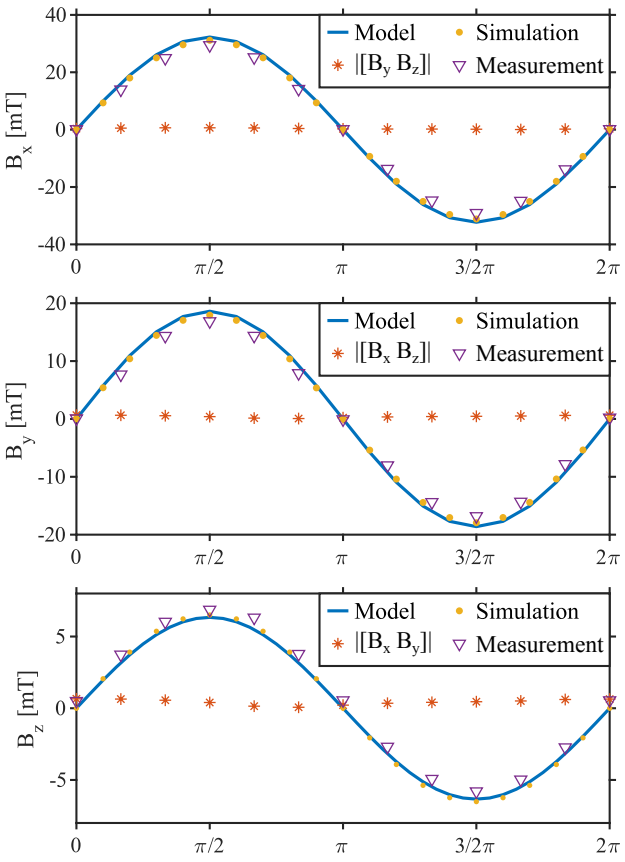

Fig. 5: Experimental measurements, finite-element-method predictions, and analytical model predictions of single-axis oscillating magnetic fields at the workspace center. For the magnetic fields (B_x, B_y) in x and y-direction of frame $\{T\}$, the paired magnets counter-rotate with an initial 180° offset while coil current $I = 0$ A. For the field (B_z) in z-direction of $\{T\}$, the magnets are fixed and the coil current is swept ($I \in [-4, 4]$ A).

IV. System Validation

In this section, we validate our field model and demonstrate the field-shaping capabilities of HybNetic. For all experiments and demonstrations, the field is controlled by an operator in an open-loop manner.

A. Independent Field Control

We validate the simulation and analysis models by generating uniaxial magnetic fields along each Cartesian axis. For the oscillating fields in x- and y-direction of $\{T\}$, the permanent magnets start at $\varphi_{1,2,3,4} = [90°, 270°, 90°, 270°]$ and $\varphi_{1,2,3,4} = [0°, 180°, 0°, 180°]$ and then counter-rotate symmetrically with the coil current set to zero. For the oscillating field in z-direction the magnets remain at $\varphi_{1,2,3,4} = [0°, 180°, 0°, 180°]$, and the coil current follows a sinusoid. Fields are measured at the workspace center with a 3MH3A Teslameter (SENIS AG, Switzerland).

Model accuracy is evaluated using normalized root-mean-square error between measured and predicted fields. The FEM model deviates by 5.4%, 5.7%, and 8.5% on the x-, y-, and z-axes of frame $\{T\}$, respectively. The analytical

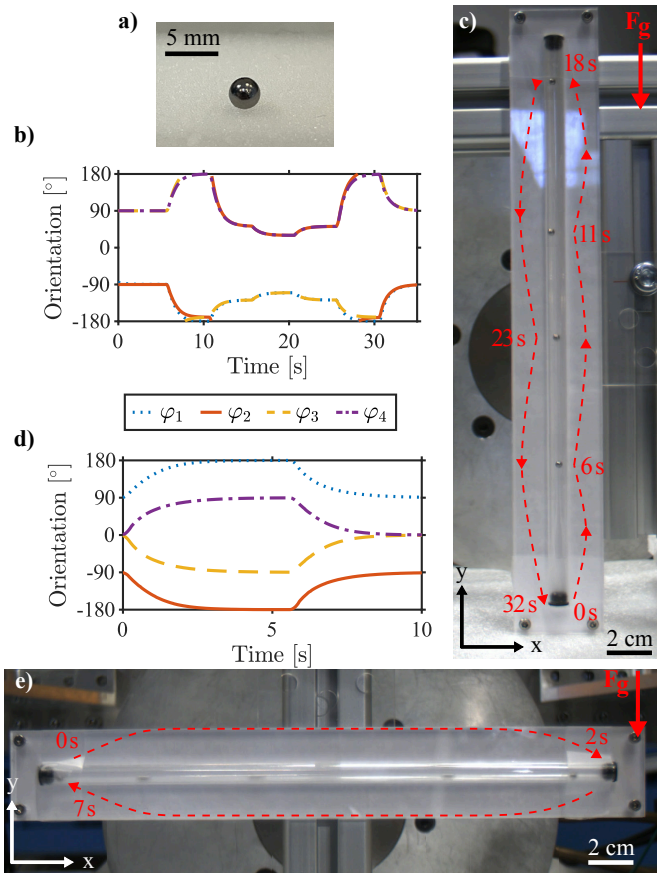

Fig. 6: Demonstration of bidirectional force application and capability to levitate a sphere against gravity ($\mathbf{F}_g$). **a)** ∅3 mm-magnetic sphere. **b)** Recorded magnet orientations $(\varphi_1, .., \varphi_4)$ for levitating the sphere. **c)** Sphere levitating at different positions. **d)** Recorded magnet orientations $(\varphi_1, .., \varphi_4)$ for bidirectional force control. **e)** Sphere moving between two positions. *Please refer to Supplementary Video for the full demonstration of the bead manipulation.*

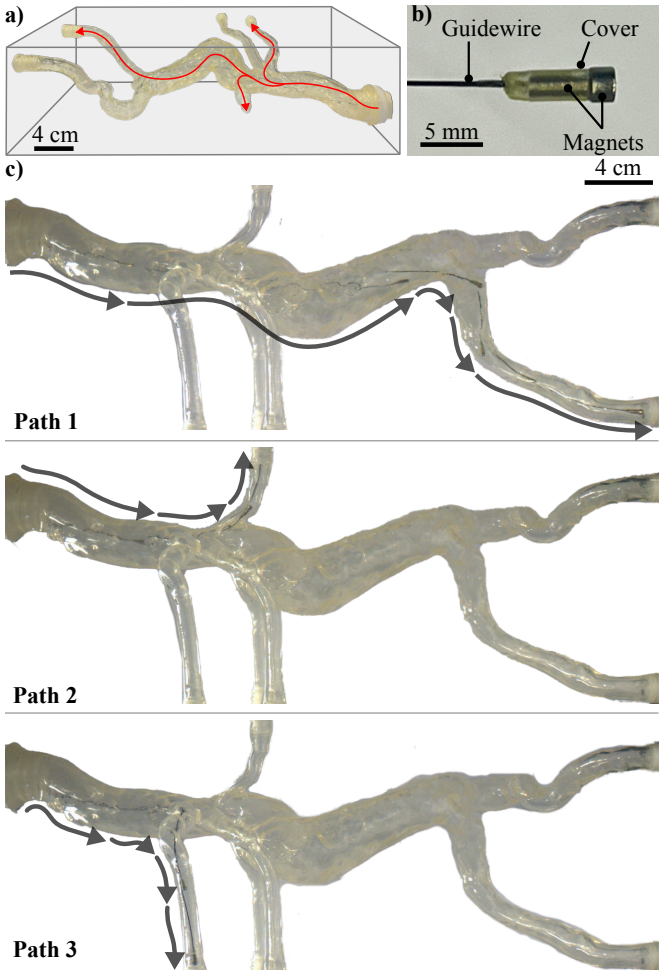

Fig. 7: Demonstration of the capability of HybNetic to steer a magnetic guidewire through a dimensionally correct phantom of the aorta with multiple branches. **a)** Size-accurate phantom of the abdominal aorta with highlighted desired paths. **b)** Magnetic guidewire. **c)** Guidewire navigation into three different branches. *Please refer to Supplementary Video for the full demonstration of the guidewire steering.*

model deviates by approximately 8.5% on each axis. The FEM model is more accurate overall because it explicitly considers the iron core and shielding plates. Along the z-axis, errors are almost identical between FEM and the analytical model, because in the analytical approach, the contribution of the coil is based on the FEM-based field mapping. The accuracy of both the FEM-based and analytical models matches the reported accuracy of state-of-the-art magnetic actuation systems [7], [15]. Across all experiments, off-axis field generation at the workspace center remained below 0.6 mT, demonstrating the capability of uniaxial field control.

B. Force-based Actuation of a Magnetic Bead

With the analytical model verified, we evaluate the force generation capability with a 3 mm NdFeB sphere. The sphere is placed in a transparent air-filled polymer tube with a 5 mm inner diameter that mimics a lumen. The motion of the sphere is constrained by the inner tube wall. Forces are evaluated along the x- and y-axes of frame $\{T\}$. The field gradient and thus the direction of force are adjusted by rotating the permanent magnets.

First, we test force generation along the x-axis of frame $\{T\}$. Initially, the sphere is attracted by one magnet pair (Fig. 6d) and 6e)). The magnetic moment of the sphere aligns with the local field and experiences a force directed towards the region of larger field magnitude. However, by using the proposed asynchronous field control approach, we can control the field gradient. By alternating the magnet's orientation between 0° and 180°, the sphere is drawn to the opposite side of the workspace, 13 cm from the center (supplementary video). This demonstrates bidirectional force control suitable for navigating magnetic microrobots across a span comparable to the diameter of a human torso.

Secondly, we test the capability of HybNetic to lift a magnetic sphere (Fig. 6b) and 6c)). The tube is mounted vertically at the workspace center with its axis aligned with the system's y-axis of frame $\{T\}$. We execute a preplanned sequence of magnet orientations derived from our analytical model. The sphere rises toward the center, then continues

upward beyond the center, traveling a total distance of $26\,\mathrm{cm}$. The sphere is held stably at intermediate heights. These results show the potential of HybNetic for moving magnetic microrobots along the body-length within constrained geometries.

C. Torque-based Actuation of a Magnetic Guidewire

After demonstrating force-based actuation, we conclude by showing the torque-based steering capabilities of HybNetic by navigating a magnetic guidewire through a dimensionally accurate silicone phantom of the abdominal aorta (Fig. 7a)). The phantom measures $40\,\mathrm{cm} \times 20\,\mathrm{cm} \times 12\,\mathrm{cm}$ and is placed at the workspace center with its longitudinal axis aligned with the y-axis of $\{T\}$. The pose of the phantom relative to the system resembles the potential clinical setting displayed in Fig. 1.

The controlled device is a custom-made magnetic guidewire (Fig. 7b)). It consists of a $0.3\,\mathrm{mm}$ commercial guidewire with two axially magnetized NdFeB magnets and a polyolefin cover. Across all trials, the insertion point of the guidewire remained fixed. The operator manually inserts the guidewire and adjusts the magnetic field under camera feedback. From the single insertion point, the guidewire was successfully navigated into three distinct aortic branches (Fig. 7c) and supplementary video). This demonstrates the controlled navigation of a surgical instrument on a human scale and highlights the suitability of HybNetic for endovascular applications in anatomically realistic environments.

V. CONCLUSIONS & FUTURE WORK

In this paper, we present HybNetic, a mobile hybrid magnetic actuation system comprising four rotatable permanent magnets and a single coil mounted on a robotic arm. The local workspace has a diameter of 520 mm and is partially surrounded by the C-shaped system. The mobility of the robot arm allows the local workspace to be repositioned flexibly, extending the effective workspace to the length of a human body. Within the local workspace, the magnetic field depends on the orientation of the individual magnets, which are controlled individually by four motors, the applied coil current and the relative position. The field generated by each magnetic source is modeled individually and superimposed into a combined model, enabling accurate field prediction required for future magnetic wrench or pose control.

We evaluate the functionality of HybNetic via three experiments covering uniaxial field control, bidirectional force generation, and navigation in an anatomically accurate phantom. Uniaxial fields are generated along each Cartesian axis with negligible off-axis components. The measured fields match the model predictions, showing the accuracy of our model. Bidirectional forces are used to move a magnetic sphere in a confined environment, successfully lifting the sphere up to 26 cm, demonstrating the potential for controlling magnetic microrobots. Finally, we navigate a guidewire through a dimensionally accurate aortic phantom to three target positions by controlling the field direction, demonstrating surgically relevant magnetic steering.

Future work will focus on the implementation of closed-loop magnetic field control using an inverse field mapping. Based on the presented field model, the inverse field mapping computes magnet angles and coil current for a desired field vector at a target position. Furthermore, control strategies will be developed that account for the transient magnetic field during magnet reorientation and that exploit the mobility of the robotic arm to shape the magnetic field. Building upon closed-loop field control, the next objective is the realization of wrench and pose control under *ex vivo* conditions, which requires reliable device localization. Here, we will investigate integration of device-based localization approaches like fiber optic shape sensing [28] or wireless sensing [29] as well as external methods such as ultrasound, which has been successfully demonstrated for localizing microrobots in tissue [30]. Finally, we will apply the system to additional anatomies such as the brain or gastrointestinal tract, and to other device classes including endoscopic capsules, soft robots, and microrobots, with emphasis on diagnostics, targeted drug delivery, and localized therapy.

REFERENCES

[1] T. Haidegger, S. Speidel, D. Stoyanov, and R. M. Satava, "Robot-Assisted Minimally Invasive Surgery—Surgical Robotics in the Data Age," *Proceedings of the IEEE*, vol. 110, pp. 835–846, July 2022.

[2] A. Handa, A. Gaidhane, and S. G. Choudhari, "Role of Robotic-Assisted Surgery in Public Health: Its Advantages and Challenges," *Cureus*, June 2024.

[3] Y. Huo, L. Yang, T. Xu, and D. Sun, "Design, Control, and Clinical Applications of Magnetic Actuation Systems: Challenges and Opportunities," *Advanced Intelligent Systems*, vol. 7, p. 2400403, Mar. 2025.

[4] Z. Yang, H. Yang, Y. Cao, Y. Cui, and L. Zhang, "Magnetically Actuated Continuum Medical Robots: A Review," *Advanced Intelligent Systems*, vol. 5, p. 2200416, June 2023.

[5] W. Chen, J. Sui, and C. Wang, "Magnetically Actuated Capsule Robots: A Review," *IEEE Access*, vol. 10, pp. 88398–88420, 2022.

[6] V. Iacovacci, E. Diller, D. Ahmed, and A. Menciassi, "Medical Microrobots," *Annual Review of Biomedical Engineering*, vol. 26, pp. 561–591, July 2024.

[7] M. P. Kummer, J. J. Abbott, B. E. Kratochvil, R. Borer, A. Sengul, and B. J. Nelson, "OctoMag: An Electromagnetic System for 5-DOF Wireless Micromanipulation," *IEEE Transactions on Robotics*, vol. 26, pp. 1006–1017, Dec. 2010.

[8] F. Ongaro, S. Pane, S. Scheggi, and S. Misra, "Design of an Electromagnetic Setup for Independent Three-Dimensional Control of Pairs of Identical and Nonidentical Microrobots," *IEEE Transactions on Robotics*, vol. 35, pp. 174–183, Feb. 2019.

[9] J. Nam, W. Lee, E. Jung, and G. Jang, "Magnetic Navigation System Utilizing a Closed Magnetic Circuit to Maximize Magnetic Field and a Mapping Method to Precisely Control Magnetic Field in Real Time," *IEEE Transactions on Industrial Electronics*, vol. 65, pp. 5673–5681, July 2018.

[10] Q. Boehler, S. Gervasoni, S. L. Charreyron, C. Chautems, and B. J. Nelson, "On the Workspace of Electromagnetic Navigation Systems," *IEEE Transactions on Robotics*, vol. 39, pp. 791–807, Feb. 2023.

[11] S. Gervasoni, N. Pedrini, T. Rifai, C. Fischer, F. C. Landers, M. Mattmann, R. Dreyfus, S. Viviani, A. Veciana, E. Masina, B. Aktas, J. Puigmartí-Luis, C. Chautems, S. Pané, Q. Boehler, P. Gruber, and B. J. Nelson, "A Human-Scale Clinically Ready Electromagnetic Navigation System for Magnetically Responsive Biomaterials and Medical Devices," *Advanced Materials*, vol. 36, p. 2310701, Aug. 2024.

[12] J. Sikorski, C. M. Heunis, F. Franco, and S. Misra, "The ARMM System: An Optimized Mobile Electromagnetic Coil for Non-Linear Actuation of Flexible Surgical Instruments," *IEEE Transactions on Magnetics*, vol. 55, pp. 1–9, Sept. 2019.

[13] L. Yang, X. Du, E. Yu, D. Jin, and L. Zhang, "DeltaMag: An Electromagnetic Manipulation System with Parallel Mobile Coils," in *2019 International Conference on Robotics and Automation (ICRA)*, (Montreal, QC, Canada), pp. 9814–9820, IEEE, May 2019.

[14] X. Du, M. Zhang, J. Yu, L. Yang, P. W. Y. Chiu, and L. Zhang, "Design and Real-Time Optimization for a Magnetic Actuation System With Enhanced Flexibility," *IEEE/ASME Transactions on Mechatronics*, vol. 26, pp. 1524–1535, June 2021.

[15] P. Ryan and E. Diller, "Magnetic Actuation for Full Dexterity Microrobotic Control Using Rotating Permanent Magnets," *IEEE Transactions on Robotics*, vol. 33, pp. 1398–1409, Dec. 2017.

[16] Z. Zhang, A. Klingner, S. Misra, and I. S. M. Khalil, "Design and control of a permanent magnet-based robotic system for navigating tetherless magnetic devices in viscous environments," *Scientific Reports*, vol. 15, p. 31041, Aug. 2025.

[17] G. Pittiglio, L. Barducci, J. W. Martin, J. C. Norton, C. A. Avizzano, K. L. Obstein, and P. Valdastri, "Magnetic Levitation for Soft-Tethered Capsule Colonoscopy Actuated With a Single Permanent Magnet: A Dynamic Control Approach," *IEEE Robotics and Automation Letters*, vol. 4, pp. 1224–1231, Apr. 2019.

[18] Y. Kim, E. Genevriere, P. Harker, J. Choe, M. Balicki, R. W. Regenhardt, J. E. Vranic, A. A. Dmytriw, A. B. Patel, and X. Zhao, "Telerobotic neurovascular interventions with magnetic manipulation," *Science Robotics*, vol. 7, p. eabg9907, Apr. 2022.

[19] G. Bassil, S. M. Markowitz, C. F. Liu, G. Thomas, J. E. Ip, B. B. Lerman, and J. W. Cheung, "Robotics for catheter ablation of cardiac arrhythmias: Current technologies and practical approaches," *Journal of Cardiovascular Electrophysiology*, vol. 31, pp. 739–752, Mar. 2020.

[20] G. Pittiglio, M. Brockdorff, T. Da Veiga, J. Davy, J. H. Chandler, and P. Valdastri, "Collaborative Magnetic Manipulation via Two Robotically Actuated Permanent Magnets," *IEEE Transactions on Robotics*, vol. 39, pp. 1407–1418, Apr. 2023.

[21] J. J. Abbott, K. E. Peyer, M. C. Lagomarsino, L. Zhang, L. Dong, I. K. Kaliakatsos, and B. J. Nelson, "How Should Microrobots Swim?," *The International Journal of Robotics Research*, vol. 28, pp. 1434–1447, Nov. 2009.

[22] Z. Yang and L. Zhang, "Magnetic Actuation Systems for Miniature Robots: A Review," *Advanced Intelligent Systems*, vol. 2, p. 2000082, Sept. 2020.

[23] J. Dirken, L. Steenbekkers, Daanen, A. Voorbij, and J. J. Molenbroek, "Dutch adults (DINED - anthropometric database)," Aug. 2018.

[24] D. Li, F. Niu, J. Li, X. Li, and D. Sun, "Gradient-Enhanced Electromagnetic Actuation System With a New Core Shape Design for Microrobot Manipulation," *IEEE Transactions on Industrial Electronics*, vol. 67, pp. 4700–4710, June 2020.

[25] A. J. Petruska, J. Edelmann, and B. J. Nelson, "Model-Based Calibration for Magnetic Manipulation," *IEEE Transactions on Magnetics*, vol. 53, pp. 1–6, July 2017.

[26] A. J. Petruska and J. J. Abbott, "Optimal Permanent-Magnet Geometries for Dipole Field Approximation," *IEEE Transactions on Magnetics*, vol. 49, pp. 811–819, Feb. 2013.

[27] J. J. Abbott, E. Diller, and A. J. Petruska, "Magnetic Methods in Robotics," *Annual Review of Control, Robotics, and Autonomous Systems*, vol. 3, pp. 57–90, May 2020.

[28] F. Khan, A. Donder, S. Galvan, F. R. Y. Baena, and S. Misra, "Pose Measurement of Flexible Medical Instruments Using Fiber Bragg Gratings in Multi-Core Fiber," *IEEE Sensors Journal*, vol. 20, pp. 10955–10962, Sept. 2020.

[29] Q. Cao, R. Deng, Y. Pan, R. Liu, Y. Chen, G. Gong, J. Zou, H. Yang, and D. Han, "Robotic wireless capsule endoscopy: recent advances and upcoming technologies," *Nature Communications*, vol. 15, p. 4597, May 2024.

[30] S. Pane, V. Iacovacci, E. Sinibaldi, and A. Menciassi, "Real-time imaging and tracking of microrobots in tissues using ultrasound phase analysis," *Applied Physics Letters*, vol. 118, p. 014102, Jan. 2021.